Dynamics of bound states of same-chirality spiral waves

Christian W. Zemlin,[1] Karthik Mukund,[1] Vadim N. Biktashev,[2] and Arkady M. Pertsov[1]
[1]*Department of Pharmacology, SUNY Upstate Medical University, Syracuse, New York 13210, USA*
[2]*Department of Mathematical Sciences, University of Liverpool, Liverpool L69 7ZL, United Kingdom*
(Received 19 December 2005; published 18 July 2006)

We describe the dynamics of bound states of same-chirality spirals in a generic numerical model of an excitable medium. For each bound state, we analyze its tip trajectory patterns and determine its characteristic frequencies. We report two previously unidentified bound states: for spiral pairs, a state that exhibits alternating cycles of small and large distances between collisions (A_2); for triplets, the first example of a meandering bound state (M_3). In parameter space, A_2 lies in between the previously described oscillating pairs (O_2) and master-slave pairs (MS). We present numerical evidence that the transition $O_2 \rightarrow A_2$ occurs via a supercritical period-doubling bifurcation, while the transition $A_2 \rightarrow MS$ occurs via a symmetry breaking secondary Hopf bifurcation. A classification of all regimes according to dynamical systems theory exposes the wealth of phenomena exhibited by multiarmed spiral waves.

DOI: 10.1103/PhysRevE.74.016207 PACS number(s): 89.75.Kd, 82.40.Ck, 05.65.+b

I. INTRODUCTION

Spiral waves occur in a variety of physical, chemical, and biological systems. Examples include the Belousov-Zhabotinsky reaction [1,2], electrical ativity in cardiac tissue [3], aggregation of starving slime mold amoeba [4], and catalytic reactions on platinum surfaces [5]. At the same time, analytical and simulation studies have greatly advanced our understanding of spiral wave dynamics [6–10].

Two or more spirals can form bound states, i.e., stable ensembles of spiral arms that interact and remain within a limited distance from each other. They have characteristic features, like their frequency [11,12], and rules of interaction with other bound states [12].

An important example of bound states are multiarmed spiral waves, ensembles of same-chirality spiral waves whose tips are separated by less than a core diameter. They have been observed in chemical media, like the Belousov-Zhabotinsky reaction [11], and in biological media, e.g., *Dictyostelium discoideum* [13], two-dimensional cultured heart tissue [14], the whole rabbit heart [15], and a variety of numerical models of excitable media [16].

The simplest type of same-chirality bound states are oscillating multiarmed spirals (O_n) [17]. They are characterized by an n-fold rotational symmetry and periodic collisions of their arms. Recently, our group discovered another bound state of two same-chirality spirals in which one spiral rotates around the other (master-slave pairs or MS) [18]. This state exhibits no symmetry, and the spiral tips are separated by a distance which can be large compared to the diameter of the core of the spiral. Finally, multiarmed spirals rotating around a common core can persist for a considerable time [13]; however, they have been shown analytically to be unstable for several FitzHugh-Nagumo type media [9] and are not included in our discussion.

While many papers have commented on the complex dynamics of bound states [11,12,14], these dynamics have not yet been analyzed. In this paper, we study the dynamics of bound states of same-chirality waves in a generic excitable medium. We report a previously unidentified stable regime of spiral pairs, in which the spiral arms alternate between larger and smaller separations between collisions (A_2). A second regime we found are triple-armed meandering spirals (M_3). We characterize the bifurcations that mark the transitions between bound states. We classify all observed regimes in terms of the theory of dynamical systems with symmetry and determine for each regime the parameter region in which it is stable. Table I summarizes the properties of the bound states of same-chirality spiral waves.

II. METHODS

A. Numerical methods

All observations were made in numerical simulations in the widely used Barkley reaction-diffusion model [19] of a generic excitable medium. It consists of an activator variable u and an inhibitor variable v, which evolve according to

$$\partial u/\partial t = (1/\varepsilon)u(1-u)[u-(v+b)/a] + \nabla^2 u,$$
$$\partial v/\partial t = u - v. \tag{1}$$

The constant ε is the ratio of characteristic time scales of the activator and inhibitor variables. The parameters a and b represent the slope of the u-nullcline and the excitation threshold. We chose a typical value of $\varepsilon=0.02$ and varied b from 0.15 to 0.3. We set $a=1.1$ unless stated otherwise (a was always between 0.9 and 1.25). All of the regimes we describe can be observed in the parameter region for which single-armed spirals rigidly rotate, so the complexity observed here is truly a consequence of the interaction of the spiral arms.

We solved the model equations on a 320×320 or 640×640 grid using Euler's method with zero flux boundary conditions, $dx=0.1826$ as our space step, and $dt=0.003$ as our time step. The tips of spiral waves were defined to be the pixels satisfying $0.45<u<0.57$ and $0<du/dt<10$. All computations were performed on a 32-node Beowulf cluster.

TABLE I. Bound states of same-chirality spiral waves. Gray background indicates bound states that are described in this paper for the first time.

Symbol	Bound state	Isotropy group	Attractor in orbit space	Figure
O_n	Oscillating multiarmed spirals with n arms	Z_n	Limit cycle	1
A_n	Alternating oscillating multiarmed spirals with n arms	Z_n	Limit cycle (double period)	2
MS	Master-slave pairs	$\{id\}$	Torus	3
M_n	Meandering multiarmed Spirals with n arms	$\{id\}$	Torus	4, 5

To create bound states of spiral waves, we used two different methods. In the first method, we initiated two consecutive plane waves, let them advance halfway through our medium. We then reset half of our medium, creating two broken wave fronts. In the second method, we superimposed snapshots of a single-armed spiral in equally spaced phases (we summed the values of each variable over the different snapshots, at each point of the medium). When we initiated bound states of three or more arms, we used the second method.

The stability of a bound state was assumed if it showed no sign of decay after at least 100 spiral rotations.

We defined the center of mass of a configuration as the center of mass of the tips. The minimal and maximal tip distances from the center were determined by automatically detecting the minimal and maximal distances for at least 10 periods and then taking the average.

To determine angular velocities in the tip trajectories (ω_1, ω_2, and ω_3; see definitions in the Results section), we measured the time needed for a large number of rotations (at least 10), and divided the covered angle by that time.

When we ramped b to study the dependence of the system's behavior on excitability, we used the final condition of each value of b as the initial condition for the next value of b and allowed transients to pass for at least 15 spiral rotations after each change in b. The boundaries of the regimes in parameter space were established with an accuracy of 0.001 in the value of b for any given a.

B. Classification of multiarmed spiral waves

A convenient language to describe the qualitative features of dynamic regimes is that of the dynamical systems theory [20]. However, this language cannot be directly applied to reaction-diffusion systems, because these systems have spatial symmetry (they are equivariant with respect to the Euclidean group, i.e., translations, rotations, and reflections). An efficient method to deal with this symmetry is to consider the space of group orbits of the system [21], which do not exhibit spatial symmetry. In this section, we explain this method without any attempt of mathematical rigor.

Consider a dynamical system defined in a phase space V and equivariant with respect to a symmetry group G. Any point $v \in V$ may have its own symmetry group $H = H(v) \subset G$ which is called the *isotropy* group of point v. The isotropy subgroup is the same for all points of a trajectory. The union of all points with similar isotropy subgroups is called a stratum. The phase space V is a disjoint union of strata. Asymmetric solutions have the trivial isotropy subgroup $\{id\}$, consisting only of the identical transformation. For the system (1), the asymmetric solutions are single-armed spirals or asymmetric multiarmed spirals.

We also consider here n-armed spiral waves, which are symmetric with respect to rotation by a multiple of $2\pi/n$. Their isotropy groups are isomorphic to the group Z_n. A group orbit is a set of points of V obtained from each other by applying various elements of G. By identifying all points belonging to the same orbit, we reduce the phase space V to the orbit space V/G. The part of the V/G corresponding to one stratum has a structure of a manifold, and is called an orbit manifold. Any trajectory in V generates a trajectory in V/G. The dynamical system in V/G is called the reduced dynamical system. It is generic in the sense that its dynamics are devoid of the original symmetry of the problem; so we can expect to find standard types of attractors and bifurcations on that system, unlike the original.

For system (1) and G the Euclidean group, in some cases the reduced dynamical system can be understood as system (1) rewritten in a moving frame of reference, say attached to the tip of a spiral [22]. Thus we will sometimes refer to (1) as dynamics in the laboratory frame of reference.

An important technical comment in [23] is that any coordinate on the orbit manifold is a group-invariant function of the phase space of (1), and vice versa, any such function can be used as a coordinate on an orbit manifold unless it is a constant for that manifold.

To summarize, the implications important for our present study are:

(1) The understanding of the dynamic regimes of multiarmed spiral waves should be in terms of dynamics on the orbit manifolds by the Euclidean group, and this can be achieved by using Euclidean invariant functions of such solutions.

(2) The structure of the orbit manifold depends on the symmetry (the isotropy subgroup) of the solutions in question, and as long as the solutions in question are within one stratum, i.e., have the same symmetry, the dynamics on the group manifold is generic, in particular, should be expected

to demonstrate attractors and bifurcations typical for generic, nonsymmetric systems.

Moreover, by Takens' embedding theorem [24], just one such coordinate is almost certainly sufficient to reconstruct qualitatively the dynamic attractor. In our simulations, the symmetry of solutions was always evident, so no special technique for its detection was needed. As the Euclidean-invariant characteristic of two-armed spiral wave solutions we have used the distance $d(t)$ between the two tips, which was easy to measure and interpret. Then we applied to $d(t)$ the standard delayed embedding technique to reconstruct the attractors.

For symmetric three-armed solutions, we used the distance between one of the tips and the center of symmetry as the Euclidean-invariant characteristic, which is also group-invariant and practical inasmuch as the center of symmetry can be found with sufficient accuracy.

III. DYNAMICS OF THE MULTIARMED SPIRAL REGIMES

A. Oscillating pairs (O_2)

Figure 1 shows the detailed dynamics of O_2. The two spiral tips approach each other [Fig. 1(a)], collide [Fig. 1(b)], and move apart again [Fig. 1(c)]. Between collisions, both tips follow a circular trajectory of the same radius of an isolated single spiral wave [Figs. 1(c) and 1(d)], until they collide again at their tips [Fig. 1(e)]. The relative positions of the spiral arms at each collision are identical [Figs. 1(b) and 1(e)], but from one collision to the next, both arms are rotated around the center of symmetry. This second rotation explains the petal pattern [Fig. 1(f)] that the tip trajectories form over several rotations. Figure 1(g) shows the distance between the tips as a function of time. It is strictly periodic with period T.

The tip trajectories can thus be described as a combination of a steady rotation of each spiral arm around its core and periodic discrete rotations, at each collision, of the whole pair. To quantify the steady rotation, we define the petal frequency $\omega_1=2\pi/T$. The periodic rotation of the whole pair can be interpreted as a second, slower rotation: We name the angle of deflection α_2 and define the meandering frequency $\omega_2=\alpha_2/T$. After head-on collisions, we always assumed that the tips exchange their spiral arms. The reason for this convention is that for collisions away from the tip, the tips manifestly exchange arms, and with our convention, we treat all collisions equally.

The sign of ω_1 was the same as that of ω_2 in all our simulations, and we set $\omega_1, \omega_2>0$ without loss of generality (taking the mirror image of the medium changes the sign of both ω_1 and ω_2). From the definitions of ω_1 and ω_2 it follows immediately that $\omega_1>\omega_2$. We describe in the Methods section how we measure ω_1 and ω_2.

Figure 1(h) shows a recurrence map for the Poincaré cross section defined by the local maxima of $d(t)$. Since there is no discernible structure in the recurrence map and the changes in the maxima of $d(t)$ are minimal, we conclude that the attractor of O_2 in orbit space is a limit cycle, i.e., we have a

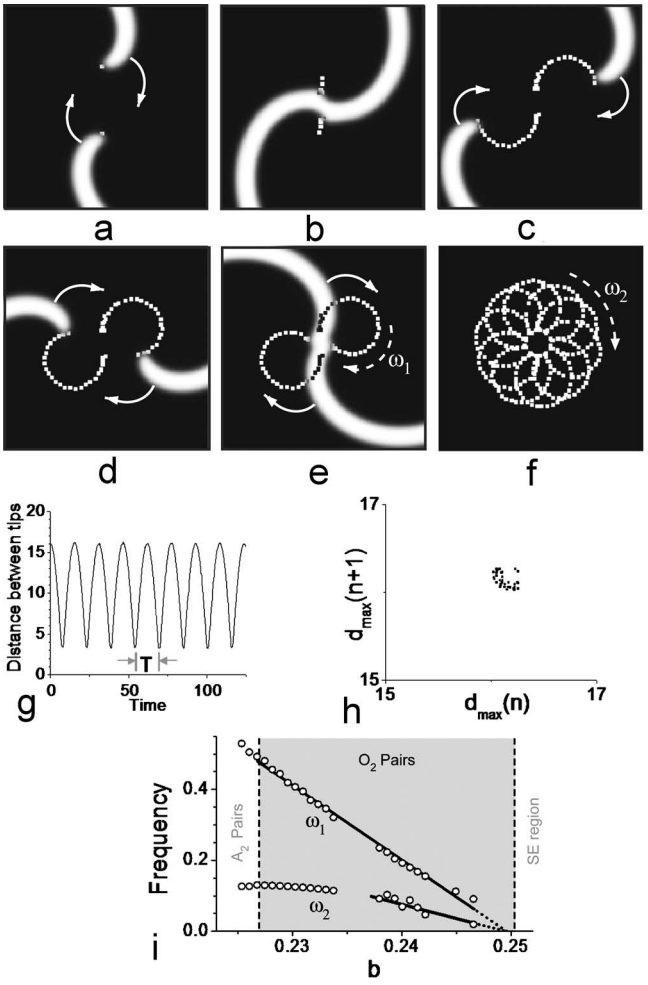

FIG. 1. Representative example of O_2 dynamics ($b=0.2303$). Thick white lines show the excitation waves ($u\approx 1$), dotted white lines show the tip trajectories. Arrows indicate the drift direction of the tips. (a)–(e) Evolution of O_2 over 1.5 periods. (f): Tip trajectories of O_2 over four periods. (g): The distance d between the tips as a function of time. (h): Recurrence map for the Poincaré cross section defined by the local maxima of $d(t)$. (i) Petal frequency ω_1 and meandering frequency ω_2, as a function of b. The O_2 region is marked gray, the adjacent regimes (A_2,SE) are discussed below.

periodic solution of the reduced system. In the laboratory frame of reference, this generates a biperiodic solution. This is similar to the classical flower-pattern meander of single-armed spirals, only here both tips describe the same flower patterns symmetrically.

Figure 1(i) shows ω_1 and ω_2 as a function of b. The dependency of ω_1 on b is in good approximation linear. Extrapolating the b for which ω_1 is 0 leads to good agreement with the largest b that supports spiral pairs (as well as single spirals). This should be expected, because the single spiral radius grows to infinity as we approach the boundary of the spiral pair domain, and consequently ω_1 should vanish. Our extrapolation of ω_2 reaches zero at practically the same value of b; this can also be expected because $\omega_1>\omega_2$ (see above). As b is decreased, ω_2 grows, but the growth saturates towards the end of the O_2 regime.

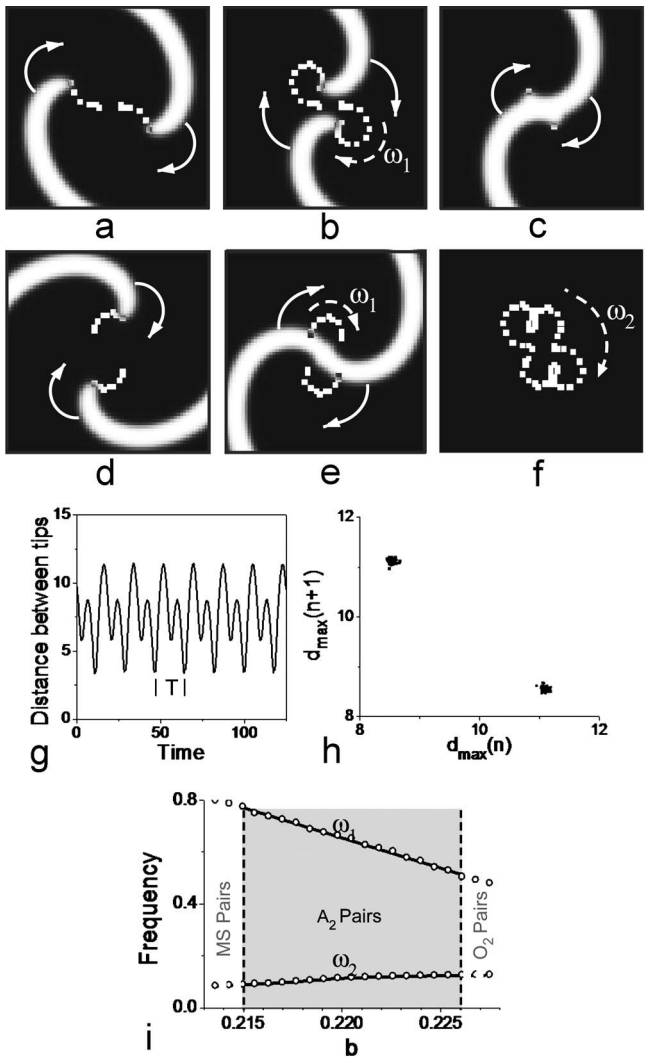

FIG. 2. Representative example of A_2 dynamics (b=0.2177). (a)–(e) Evolution of A_2 over one period. (f) Tip trajectories of A_2 over one period. (g) The distance d between the tips as a function of time. (h) Recurrence map for the Poincaré cross section defined by the local maxima of $d(t)$. (i) Petal frequency ω_1 and meandering frequency ω_2 as a function of b. The A_2 region is marked gray, the adjacent *MS* regime is discussed below.

The observed O_2 regime corresponds to the stable spiral pairs described by Ermakova *et al.* for a different FitzHugh-Nagumo medium [17].

B. Alternating pairs (A_2)

Figure 2 shows a previously unidentified, alternating regime of spiral pairs, which we call A_2. As in the case of O_2, the two spiral arms maintain perfect center (Z_2) symmetry [Figs. 2(a)–2(e)]. However, A_2 exhibits two different types of collisions that occur alternatingly. The first type of collision is "sideways." The initial contact between the two arms occurs at some distance from the tip [Fig. 2(c)]. The second type is "head-on," i.e., collision occurs close to the tip [Fig. 2(e)], as for O_2. Figure 2(f) shows that the tip trajectories in the two types of intercollision periods also differ: They form a petal pattern that contains two different petal sizes.

Figure 2(g) shows the distance between the tips as a function of time, where alternans can also clearly be seen. Figure 2(h) shows the recurrence map for the Poincaré section defined by the local maxima of $d(t)$.

The empirical attractor consists of two clusters, neither of which has any further discernible structure. We conclude that the attractor in orbit space of A_2 is a limit cycle; but this time, the period is about twice that of an isolated spiral in the same medium.

Figure 2(i) shows that the linear increase of ω_1 with decreasing b continues throughout the A_2 domain, while ω_2 begins to decrease. Note that for A_2, the period T between collisions is alternating (say, between T_1 and T_2). Thus, our definitions of ω_1 and ω_2 need to be modified to $\omega_1 = 4\pi/(T_1+T_2)$ and $\omega_2 = \alpha_2'/(T_1+T_2)$, where α_2' is the angle that the whole pair rotates during the time T_1+T_2.

From the formal viewpoint, the orbit space dynamics here are periodic, as for O_2, although the shape of the oscillations is more complicated. We will discuss the relationship between A_2 and O_2 orbit space dynamics in more detail below.

C. Master-slave pairs (*MS*)

Figure 3 shows a third regime of double-armed spiral waves (*MS*), in which the central symmetry is broken. The spiral tip that is to the left in Fig. 3(a) rotates apparently unaffected by the collisions through the entire sequence shown in Figs. 3(a)–3(f). At the same time, the other tip is annihilated in every collision [Figs. 3(b) and 3(e)] but develops again afterwards [Fig. 3(c)]. We call the spiral that belongs to the unaffected tip "master" and the other spiral "slave." The master takes over the slave arm after each collision, and the slave redevelops from the truncated master arm. Panel (f) shows master and slave tip trajectories. The distance between master and slave, averaged over one collision period, converges to its steady state within a few revolutions of the slave around the master.

Figure 3(g) shows that the distance between the tips is in a good approximation periodic, but that the extrema vary slightly from beat to beat.

This variation is further analyzed in Fig. 3(h), which shows the recurrence map for the Poincaré section defined by the local maxima of $d(t)$. The recurrence map forms a closed loop, and we conclude that the attractor in orbit space of *MS* is a torus. In Fig. 3, we show the recurrence map for b =0.2214, because the loop is more pronounced for larger b, for which master and slave are close together [Fig. 3(i) suggests that b=0.2214 does not support *MS*, but there is actually MS/A_2 bistability for b=0.2214, as we discuss below, in Fig. 9].

In Fig. 3(i), we see that ω_1 continues to grow as b decreases. On the contrary, ω_2 approaches zero as we approach the left end of the *MS* domain. This is because the master-slave distance diverges towards the left end of the *MS* domain while the petal size (like the radius of an isolated spiral) decreases.

D. Meandering triplets (M_3)

We now turn to spirals with three arms. Figure 4 shows the dynamics of a triple-armed, meandering spiral wave

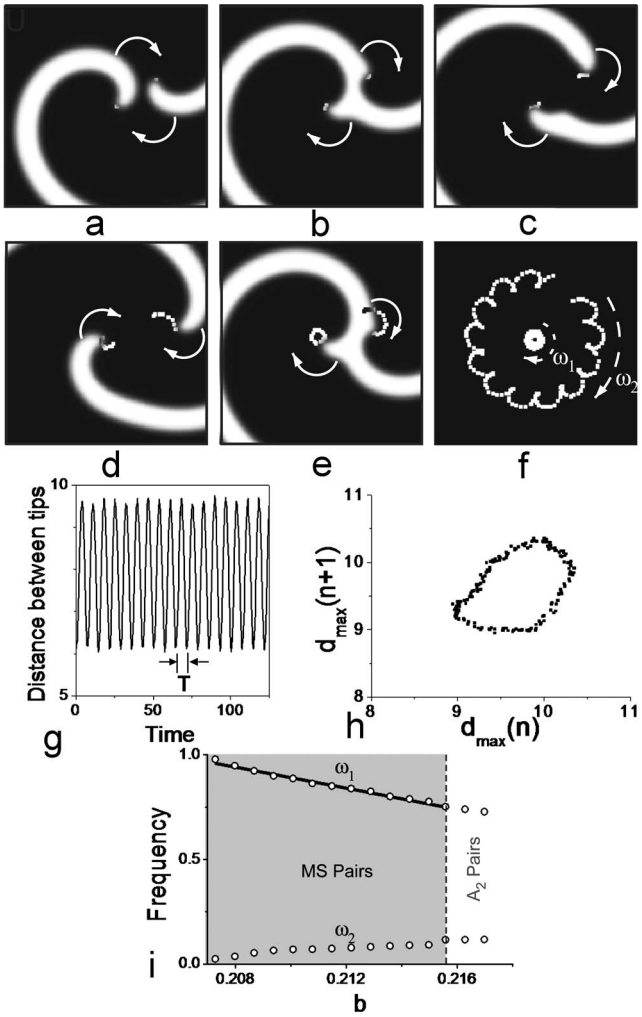

FIG. 3. Representative example of *MS* dynamics ($b=0.2087$). (a)–(e) Evolution of *MS* over one period. (f) Master and slave tip patterns for one complete revolution of the slave around the master. (g) The distance d between the tips as a function time. (h) Recurrence map for the Poincaré cross section defined by the local maxima of $d(t)$. For this panel, we used $b=0.2214$ (see text). (i) Petal frequency ω_1 and meandering frequency ω_2 as a function of b.

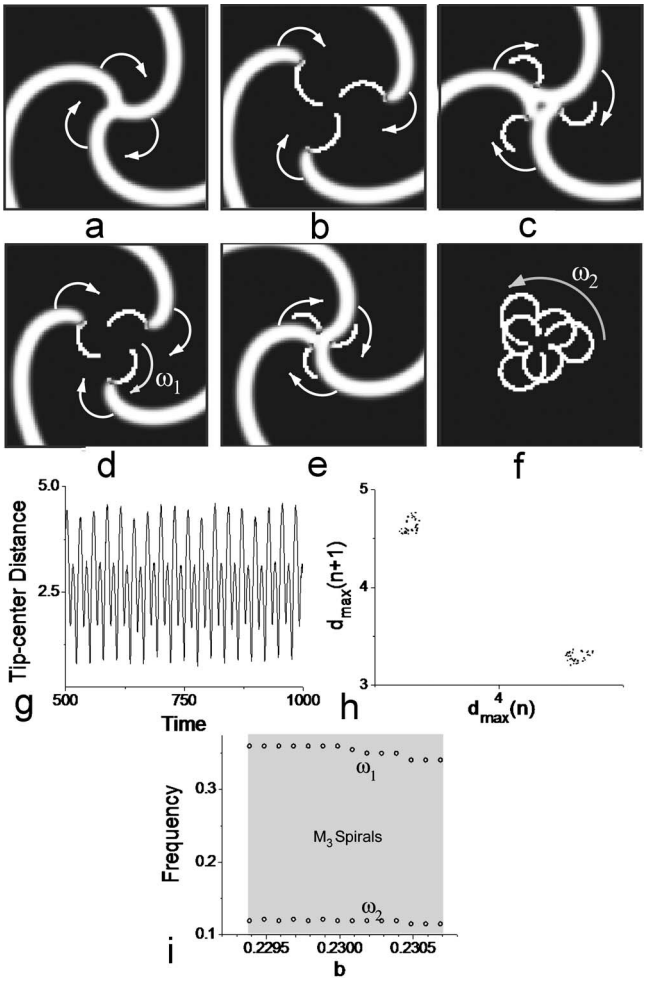

FIG. 4. Representative example of M_3 dynamics ($a=1.25$, $b=0.27488$). (a)–(e) Evolution of stable triple-armed spirals over two periods. We observed two types of collisions, which alternate every rotation cycle: head-on collisions [frames (a),(e)], and sidearm collisions [frame (c)]. (f) Tip trajectory of a triple-armed spiral over two periods. The alternating tip and sidearm collisions form two concentric patterns. (g) Distance d from the tips to the center as a function of time (equal for all three arms). (h) Recurrence map for the Poincaré cross section defined by the local maxima of $d(t)$. (i) Petal frequency ω_1 and meandering frequency ω_2 as a function of b.

(M_3). Apart from its meandering, the configuration is analogous to A_2: Between collisions, the individual tips move along circular trajectories, as independent single arms. There are two types of collisions that occur alternatingly: head-on [Figs. 4(a) and 4(e)] and sideways [Fig. 4(c)]. The tip trajectories also form a pattern analogous to that of alternating spiral pairs, characterized by a small petal radius and a big petal radius [Fig. 4(f)].

Figure 4(g) shows the tip distance over time, reflecting the alternating motion. Figure 4(h) shows the recurrence map for the Poincaré section defined by the local maxima of $d(t)$. The recurrence map shows two closed loops, so it provides evidence that the attractor in orbit space of M_3 is a torus. However, the structure of the loops is not clear enough to rule out a more complicated attractor, e.g., a 3-torus, which is suggested by the observation of meander discussed below.

Figure 4(i) shows the petal frequency (ω_1) and the meandering frequency (ω_2) as a function of b. Both ω_1 and ω_2 remain almost constant over the A_3 domain (which is relatively small).

Figure 5(a) shows that the whole triplet meanders on a circular path. The amplitude of the meandering is comparable to the core diameter of an isolated spiral. We define the angular meandering velocity $\omega_3=2\pi/T_3$, where T_3 is the period of the meandering [see Fig. 5(b)]. The frequency ω_3 depends on b (such as ω_1 and ω_2), and it is consistently lower than ω_2 by an order of magnitude (we have not determined the detailed dependency of ω_3 on b because of the very long duration of the corresponding simulations). Figure 5(b) shows the x and y coordinates of the center of mass (x_{COM} and y_{COM}) for a representative example of M_3. Despite some noise from tip misdetections, Fig. 5(b) shows that both coordinates oscillate sinusoidally with great accuracy.

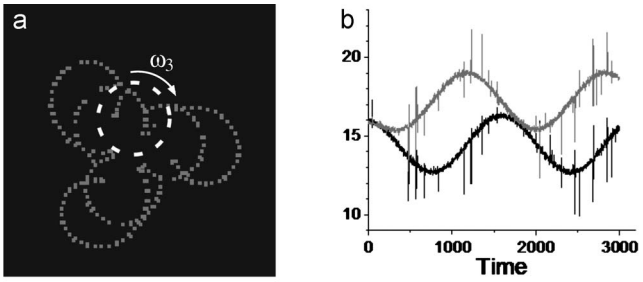

FIG. 5. Representative example of a meandering multiarmed spiral (a=1.2, b=0.262). (a) Tip trajectories and meandering. The dotted gray lines mark the tip trajectories of all three tips, the solid white dot marks the corresponding center of mass of the tips. Over time, the center of mass moves along the circle marked by a dashed white line, with angular velocity ω_3. (b) Coordinates of the center of mass as a function of time. The black trace shows the x coordinate of the center of mass (x_{COM}), the gray trace the y coordinate (y_{COM}). Noise in both traces is due to tip misdetections.

Different from the previously discussed regimes, M_3 was stable only for a narrow range of parameters and initial conditions. In the vicinity of this narrow range, M_3 can persist for a long time (>50 rotations) before developing asymmetries and finally decaying. This raises the possibility that M_3 is nowhere truly stable, but only has very large decay times for certain parameters. While we cannot rule out this possibility, we ran simulations with up to 500 spiral rotations without seeing any sign of breakup. Even if M_3 should not be analytically stable, it persists for so long that it can be considered stable for many practical purposes.

E. Parameter regions of the dynamic regimes

Figure 6 shows the parameter regions of all dynamical regimes discussed in this paper. They all lie inside the region in which a single spiral is stable (marked "SS"). O_2 occurs at highest b (lowest excitabilities), A_2 at lower b, and MS at

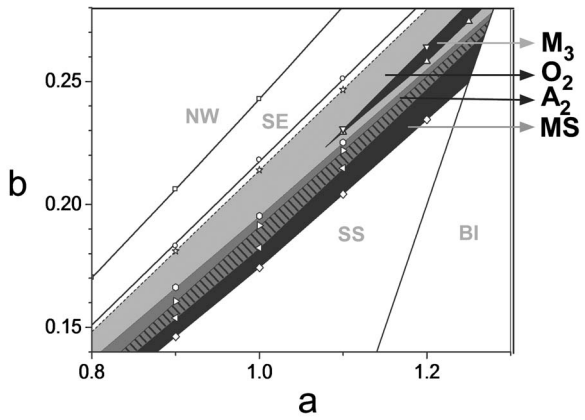

FIG. 6. Parameter regions of the dynamic regimes of the Barkley model. Light gray area marks the O_2 regime, medium gray area the A_2 domain, and black area the MS domain. The hatched area marks the overlap of the A_2 and the MS domain. Previously identified regimes are labeled in gray: NW (no waves), SE (subexcitable), SS (stable spirals), and BI (bistable).

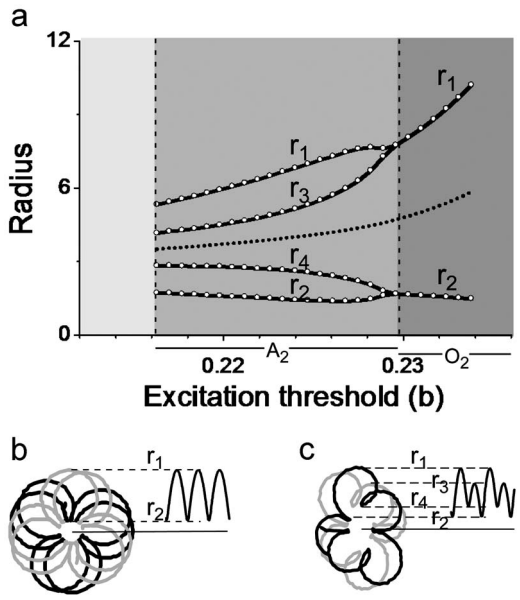

FIG. 7. Transition from O_2 to A_2 as b is changed (a=1.1). (a) Bifurcation diagram. The symbols r_1, r_2, r_3, and r_4 correspond to the external points of the tip trajectories [see panels (b) and (c)]. The dark gray area marks the range of b supporting O_2, the medium gray area the range of b supporting A_2. The light gray area marks the region of b that supports MS but not A_2 (see Fig. 8). The dotted line indicates the average distance of the spiral tips from the center of symmetry. (b) Tip trajectories of both spiral arms (gray and black) for O_2. Maximum and minimum distances between tips and the center of symmetry are labeled r_1 and r_2. (c) Tip trajectories for A_2. Additional local maxima and minima are labeled r_3 and r_4.

still lower b. Figure 6 shows that stable bound pairs cover a large portion of parameter space, i.e., more than 50% of the stable spiral (SS) domain shown in Fig. 6 (but note that the SS domain extends beyond the part of the model's parameter space shown in Fig. 6 [25]). The domain of symmetric triple armed spirals is much smaller (about 2% of the SS domain shown in Fig. 6).

We also looked for stable bound states with four arms, but they consistently broke up after a short time (10 rotations). Stable bound pairs also occurred for parameters outside the range shown in Fig. 6 (e.g., for a=0.6, b=0.08). We never observed them, however, for parameters at which a single spiral meanders [25].

IV. TRANSITIONS BETWEEN THE REGIMES

A. Transition $O_2 \rightarrow A_2$

Figure 7 shows the transition from O_2 to A_2. Figure 7(a) shows that starting from the largest value shown (b=0.234), decreasing b decreases r_1 [maximal distances of the spiral tips from the center of symmetry, see Fig. 7(b)] and increases r_2 [minimal distances of the spiral tips from the center of symmetry, right before a collision, see Fig. 7(b)]. The decrease in r_1 reflects the decrease of a single spiral's radius with b, and the growth in r_2 indicates that the spirals are meeting less and less exactly head on.

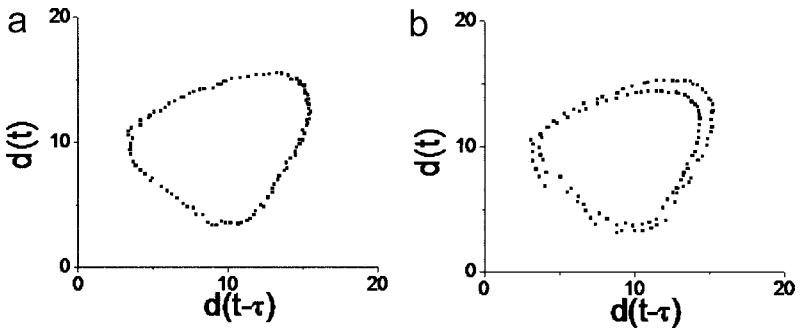

FIG. 8. Delay-embedded trajectories before [panel (a), $b=0.233$] and after [panel (b), $b=0.226$] the period doubling bifurcation. The delay τ was chosen to be $T/4$ (T measured before the bifurcation).

At $b_{O2\to A2}\approx 0.229$, a period doubling bifurcation occurs in the base system. For $b<b_{O2\to A2}$, during one period, r does not simply oscillate between r_1 and r_2, but it increases from r_2 to r_1, then decreases to r_4, increases to r_3 and decreases back to r_2 [see Fig. 7(c)]. The average radius $[r_1+r_2+r_3+r_4]/4$, shown by a dotted line in Fig. 7(a), decreases monotonically down to the end of the alternating pairs domain ($b_{A2\to MS}\approx 0.216$).

Figure 8 gives evidence that the transition $O_2\to A_2$ is indeed a period doubling bifurcation. Figure 8(a) shows the delay-embedded distance between the tips for $b=0.233$, i.e., in the O_2 domain but close to $b_{O2\to A2}$. The trajectory is a closed loop. Figure 8(b) shows the corresponding trajectory for $b=0.226$, in the A_2 domain. The closed loop has split in a double loop, but the shape is still very similar to that of Fig. 8(a). This strongly suggests that a period-doubling bifurcation occurred.

B. Transition $A_2\to MS$

Figure 9 shows the transition from A_2 to MS. In order to characterize the change in MS dynamics for different b, we introduce the slave precession radius r_s and the master precession radius r_m [Fig. 9(b)]. Figure 9(a) shows that as b is decreased below $b_{MS\to A2}\approx 0.223$, the medium begins to sustain MS (the name $b_{MS\to A2}$ will become clear in the next paragraph where we discuss hysteresis). The values of r_s and r_m are on either side of the corresponding average tip-center distance of the A_2 regime (dotted line). While r_s grows monotonically and eventually diverges at $b=0.2057$, r_m decreases monotonically and approaches zero as r_s diverges [18].

Note that there is an overlap of the A_2 and the MS domains. In the bistable region, the initial condition determines whether A_2 or MS develops. If b is varied continuously, there is hysteresis: Starting with A_2 and decreasing b slowly, the alternating pair persists down to $b_{A2\to MS}\approx 0.216$, while starting with MS and increasing b slowly, MS persists up to $b_{MS\to A2}\approx 0.223$.

Below $b_{A2\to MS}$, MS is the only stable formation. For decreasing b, the slave precession radius increases and eventually diverges around $b=0.2057$ [18] while the master precession radius converges to zero.

Note that the transition from A_2 to MS is a transition from a limit cycle to an invariant torus in the reduced system. Recall that such a transition is a typical codimension one event in generic dynamical systems, marked by a secondary Hopf bifurcation, also known as Neimark-Sacker bifurcation. In our case this is a symmetry-breaking bifurcation, as different branches correspond to different strata: A_2 has central symmetry Z_2, whereas MS has the trivial symmetry $\{id\}$. Besides, this bifurcation appears subcritical, which gives rise to the "hard" birth of the 2-torus and the hysteresis.

V. ROBUSTNESS OF MULTIARMED SPIRAL REGIMES

We performed additional simulations to demonstrate that the regimes described are robust against noise and perturbations and independent of initial conditions.

Figure 10 illustrates the reversibility of the effect of parameter changes. Figure 10(a) shows the tip trajectories for a value of b that corresponds to O_2. Then b is abruptly increased such that the spiral pair remains in the O_2 regime, but the resulting tip trajectory pattern has a smaller radius [Fig. 10(b)]. Afterwards, we set b back to its original value and get the original tip trajectory, up to a shift and a rotation [Fig. 10(c)].

Transitions between different pairs of regimes are reversible in the same manner. Figures 10(d)–10(f) illustrate this finding in the case of the regimes MS and O_2 Figure 10(d) shows a MS tip trajectory. When we abruptly increase b, the system converges to the O_2 tip trajectory pattern shown in Fig. 10(e). When we set b back to its original value, the system evolves back to the MS regime and the original tip pattern [Fig. 10(f)].

We conducted further tests of the robustness of all reported regimes. Figure 11 shows the effect of noise on MS. Figure 11(a) shows the tip trajectories of a master-slave pair before noise is switched on. In Fig. 11(b), the noise is off initially, but it is switched on when the slave tip is at the point indicated by the arrow. As soon as the noise is turned on, the slave trajectory becomes irregular; but qualitatively, the MS dynamics are preserved. The master trajectory is also affected: As soon as the noise is switched on, the master tip starts to meander randomly on top of its circulating motion. In Fig. 11(c), the noise has been turned off again, and a regular MS tip pattern sets in immediately. We show in gray the original MS tip pattern [from Fig. 11(a)], and see that the only lasting effect of the noise application is a small shift of the entire tip trajectory pattern.

We found that the steady state to which the system evolves is generally not sensitive to the initial conditions (exceptions to this rule are discussed below). Initiating any of the reported regimes in two different ways (see Methods

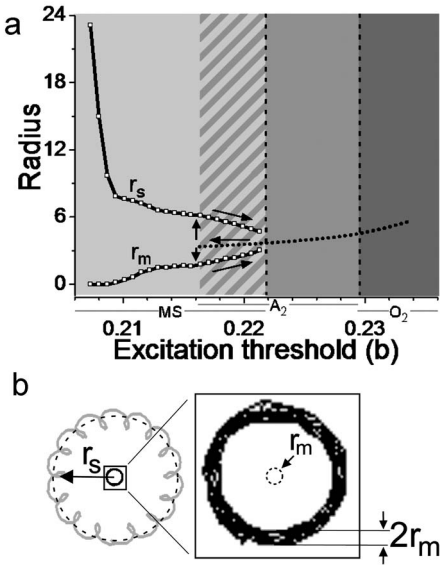

FIG. 9. Transition from A_2 to MS as b is changed (a=1.1). (a): Bifurcation diagram for r as b is changed. The symbols used are explained in panels (b) and (c). The solid lines show r_s and r_m as function of b. The dotted line indicates the average distance of the spiral tips from the center of symmetry (copied from Fig. 7). Arrows indicate which stable branch the system follows for increasing and decreasing b. There is hysteresis in the transition. The dark gray area marks the range of b supporting O_2, the medium gray area the range of b supporting A_2, and the light gray area the region b that supports MS; note the overlap of the MS and A_2 domains (hatched area). (b): Precession of the slave and master. Left panel shows the tip trajectories of slave (gray) and master (black). The motion of the slave tip is a combination of a single spiral rotation and a low-frequency precession of amplitude r_s caused by the interaction. The dashed circle marks the precession component of the trajectory. The trajectory can be recovered by moving the core center along the dashed circle as the tip rotates around the core. In the right panel, we show the magnified master tip trajectory, which appears thick because the motion of the master tip is also a combination of a single spiral rotation and a low-frequency precession of (low) amplitude r_m. The dashed circle in the center of the master tip trajectory (radius r_m) shows the precession component of the master trajectory. The thickness of the slave trajectory is $2r_m$ because this is how much the instantaneous center of the master rotation changes due to precession.

section) resulted in an identical steady state (up to a shift and a rotation). Ramping the parameter b led to the same result. Triple-armed spirals did not develop from a train of three consecutive broken waves.

We further applied one-time global additive perturbations of varying amplitude and spatial frequency to the activator variable. These perturbations did not destroy the regimes' dynamics and had a negligible effect on their phase, even for perturbation amplitudes of 0.9 activation thresholds (no figure shown).

The size of the medium and boundary conditions were relevant only if one of the tips got close to the boundary (when the distance became less than the core diameter of an isolated spiral).

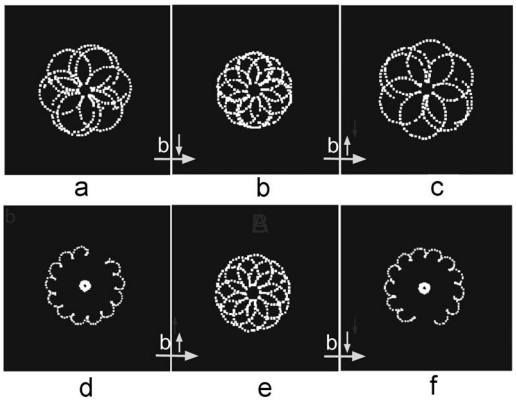

FIG. 10. Reversibility of the effect of parameter changes. (a)–(c) Parameter changes within a dynamic regime (O_2). (a) O_2 tip trajectory (b=0.2338). (b) Steady-state tip trajectory of the same spiral pair after b is decreased to 0.2303. (c) After b is decreased to its original value, the original tip pattern is restored. (d)–(f). Parameter changes across regimes. (d) MS tip trajectory (b=0.2149). (e) Increasing the value of b to 0.2303, we obtain O_2 (f) After decreasing the value of b back to 0.2149, the original O_2 is restored.

While the steady state is generally not sensitive to initial conditions, there are some exceptions. One example is the bistability shown in Fig. 7; in this part of parameter space, some initial conditions lead to A_2 and others to MS. Another example is shown in Fig. 12: MS will develop from a pair of wave breaks only if they are sufficiently close together [Figs. 12(a)–12(c)], but not if their separation is above a certain threshold [Figs. 12(d)–12(f)].

Figure 12(g) shows the evolution of the tip distance for different initial separations. For initial separations below a threshold θ ($\theta \approx 15$), the tip distance relaxed monotonously to that of a MS pair, d_{MS} ($d_{MS} \approx 10$). For initial separations larger than θ, we observe qualitatively different dynamics: The tip distance first drops below d_{MS} ("undershoot"), and then relaxes to d_{MS}. Interestingly, the relaxation to MS occurs faster for an initial separation that lies slightly above θ than for one that lies slightly below θ. However, as the initial separation is further increased, the formation time for a MS pair grows dramatically. Figure 12(h) shows how the formation time of a MS pair depends on the initial separation in a semilogarithmic plot. Formation was considered to occur when the tip distance enters the interval $d_{MS} \pm 5\%$ and stays in this interval. The data points deviate upwards from a straight line; therefore, the formation time either grows superexponentially or there is some threshold separation above which the two spiral arms do not interact.

VI. DISCUSSION

In a generic numerical model of an excitable medium, we discovered two alternating bound states (A_2 and M_3) of spiral waves. We observed the time meandering in multiarmed spirals (M_3). We showed the detailed dynamics of A_2, M_3, and the two other types of bound states that occur in this model (O_2 and MS). We scanned the parameter space and deter-

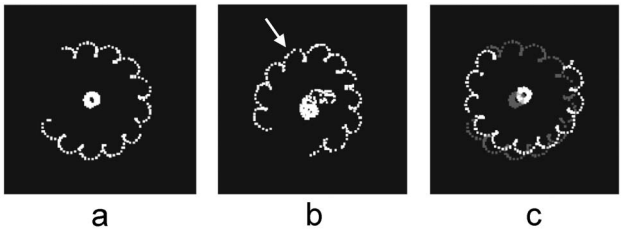

FIG. 11. Effect of random noise on *MS*. (a) Tip trajectories of master and slave before noise was switched on. (b) Transition from noise-free to noise *MS* dynamics. The arrow marks the position in the slave trajectory where the noise was turned on. The master trajectory deviates visibly from its original circular path as soon as the noise is switched on. (c) Tip trajectories after the noise has been turned off. In the background (gray) we show the original trajectories from panel (a) (notice the shift of the entire trajectory pattern). The noise applied consisted of uniformly distributed random numbers with amplitude of ±7.5% of the activation threshold, added in every time step.

mined the domains of A_2, O_2, and *MS*. Each domain occupies a significant portion of parameter space.

We have presented numerical evidence that the transition $O_2 \rightarrow A_2$ occurs via a supercritical period-doubling bifurcation in the reduced system, while the transitions $A_2 \rightarrow MS$ occurs via a symmetry breaking secondary Hopf bifurcation in the reduced system, from the Z_2 stratum to the $\{id\}$ stratum. The $O_2 \rightarrow A_2$ period doubling bifurcation is supercritical, thus the birth of the alternating spirals is "soft." On the contrary, the $A_2 \rightarrow MS$ secondary Hopf-bifurcation is subcritical, thus the small 2-tori are born unstable, the transition to the new regime is hard, and there is hysteresis.

While we analyzed the prevalence of bound states in a large portion of the parameter space, our analysis was limited to states that exhibit strict synchronization of the arms. There are other regimes in our model as well as in other models that lack such synchronization [12,16]. The detailed dynamics of these regimes have not yet been studied and are likely to be more complex.

Our simulations were naturally limited in time, and the regimes that persisted in our simulations may not be analytically stable but decay at a later time. This possibility seems most likely in the case of M_3 which was stable in our simulations only in a narrow range of parameters and initial conditions. In any case, the bound states presented here persist over very long periods and can be considered stable for many practical purposes.

Experimental data on multiarmed spirals exhibit a striking overall resemblance with our numerical simulations. In the Belousov-Zhabotinsky reaction, double- and triple-armed spirals have been observed to periodically move apart and back together [11], much like our double-armed (Figs. 1–3 and triple-armed (Figs. 4 and 5) spirals. Unfortunately, available experimental data do not yet include detailed tip trajectories or bifurcation analyses, and we do not know whether

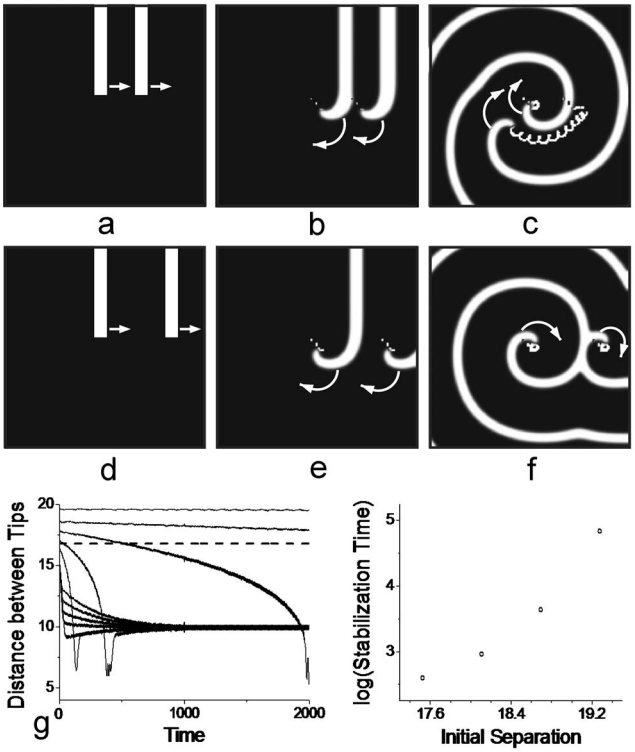

FIG. 12. Initiation of *MS* from two closely spaced wave breaks. (a)–(c) If the distance between the wave breaks is below some critical value, they develop into *MS*. (d)–(f) If the wave breaks are too widely spaced, they develop into two independent spirals. (g) Evolution of tip distance for different initial distances. The dashed line marks the single spiral wavelength. (h) Time for *MS* formation as function of initial separation of the wave fronts.

the regimes and transitions we described here occur in experimental systems as well.

Our data suggest, however, that at least some of the bound states we described and the transitions between can be observed in experiments. On the one hand, most of them occupy a significant portion of parameter space, on the other hand, they are robust against various types of perturbations. The chances may be particularly good in media whose experimental parameters can be controlled, as the Belousov-Zhabotinsky reaction. In this reaction, the excitation threshold is perfectly controllable and multiarmed spirals have already been observed [11].

ACKNOWLEDGMENTS

Research in this paper has been supported by AHA Grant No. 0325458T, by NIH Grant Nos. 5P01HL039707, 5R01HL071635, and 5R01HL071762, by NSF Grant No. CTS-0319555, and by EPSRC Grant No. EP/D500338/1 (UK). We thank Rebecca Smith and Arvydas Matiukas for carefully reading the manuscript.

[1] A. N. Zaikin and A. M. Zhabotinsky, Nature (London) **255**, 535 (1970).
[2] A. T. Winfree, Science **175**, 634 (1972).
[3] J. M. Davidenko *et al.*, Nature (London) **355**, 349 (1992).
[4] K. J. Lee, E. C. Cox, and R. E. Goldstein, Phys. Rev. Lett. **76**, 1174 (1996).
[5] M. Bär, I. G. Kevrekidis, H. H. Rotermund, and G. Ertl, Phys. Rev. E **52**, R5739–R5742 (1995).
[6] V. Zykov, *Simulation of Wave Processes in Excitable Media* (Manchester University Press, Manchester, 1984).
[7] A. Mikhailov, *Foundations of Synergetics I*, 2nd edition (Springer, New York, 1994).
[8] A. V. Panfilov and A. V. Holden, *The Computational Biology of the Heart* (Wiley, Chichester, 1997).
[9] V. Hakim and A. Karma, Phys. Rev. E **60**, 5073 (1999).
[10] F. H. Fenton, E. M. Cherry, H. M. Hastings, and S. J. Evans, Chaos **12**, 852 (2002).
[11] K. I. Agladze and V. I. Krinsky, Nature (London) **296**, 424 (1982).
[12] R. M. Zaritski and A. M. Pertsov, Phys. Rev. E **66**, 066120 (2002).
[13] B. Vasiev, F. Siegert, and C. Weijer, Phys. Rev. Lett. **78**, 2489 (1997).
[14] N. Bursac, F. Aguel, and L. Tung, Proc. Natl. Acad. Sci. U.S.A. **101**, 15530 (2004).
[15] T. J. Wu, M. A. Bray, C. T. Ting, and S. F. Lin, J. Cardiovasc. Electrophysiol. **13**, 414 (2002).
[16] R. Zaritski, J. Ju, and I. Ashkenazi, Int. J. Bifurcation Chaos Appl. Sci. Eng. 15, (in press).
[17] E. A. Ermakova, A. M. Pertsov, and E. E. Shnol, Physica D **40**, 185 (1989).
[18] C. W. Zemlin *et al.*, Phys. Rev. Lett. **95**, 098302 (2005).
[19] D. Barkley, M. Kness, and L. S. Tuckerman, Phys. Rev. A **42**, 2489 (1990).
[20] Y. A. Kuznetsov, *Elements of Applied Bifurcation Theory*, 2nd edition (Springer, New York, 1998).
[21] V. S. Afraimovich, V. I. Arnold, Y. W. Il'yashenko, and L. P. Shilnikov, *Dynamical Systems-5* (Springer, Berlin, 1984).
[22] V. N. Biktashev, A. V. Holden, and E. V. Nikolaev, Int. J. Bifurcation Chaos Appl. Sci. Eng. **6**, 2433 (1996).
[23] P. Chossat, Acta Appl. Math. **70**, 71 (2002).
[24] F. Takens, *Dynamical Systems and Turbulence* (Warwick, 1980).
[25] S. Alonso, F. Sagues, and A. S. Mikhailov, Science **299**, 1722 (2003).